

Heliosphere in the Local Interstellar Medium

Nikolai V. Pogorelov^{id}

Department of Space Science and Center for Space Plasma and Aeronomic Research,
University of Alabama in Huntsville, Huntsville, AL 35805, USA
email: np0002@uah.edu

Abstract. The Sun moves with respect to the local interstellar medium (LISM) and modifies its properties to heliocentric distances as large as 1 pc. The solar wind (SW) is affected by penetration of the LISM neutral particles, especially H and He atoms. Charge exchange between the LISM atoms and SW ions creates pickup ions (PUIs) and secondary neutral atoms that can propagate deep into the LISM. Neutral atoms measured at 1 au can provide us with valuable information on the properties of pristine LISM. *Voyager* 1 and 2 spacecraft perform in situ measurements of the LISM perturbed by the presence of the heliosphere and relate them to the unperturbed region. We discuss observational data and numerical simulations that shed light onto the mutual influence of the SW and LISM. Physical phenomena accompanying the SW–LISM interaction are discussed, including the coupling of the heliospheric and interstellar magnetic field at the heliopause.

Keywords. Sun: solar wind, ISM: kinematics and dynamics, ISM: magnetic field

1. Introduction

The interaction of the solar wind (SW) with the local interstellar medium (LISM) is a natural laboratory that allows the space physics and astrophysics communities to investigate a number of interesting physical phenomena in partially ionized plasma. Although the interaction of two plasma streams seems to be a trivial problem in the MHD sense, this is not so because the density of neutral hydrogen (H) atoms in the LISM surrounding the heliosphere is maybe three times higher than that of protons. While a tangential discontinuity, called the heliopause (HP), is formed in the ionized component, the interstellar neutral (ISN) atoms are able to penetrate deep into the heliosphere. The interaction of the ISN atoms with the SW ions occurs predominantly through the resonant charge exchange. As a result of such interaction, new neutral atoms are born with the properties of the parent SW ions and new ions with the properties of the parent ISN atoms. Newly born (secondary) neutral atoms and ions have properties strongly dependent on where in the heliosphere they were created. The flow of SW ions at distances exceeding 10–15 solar radii is super-fast magnetosonic, so its deceleration by the HP and LISM counter-pressure in the heliotail creates a heliospheric termination shock (TS). Thus, the secondary neutral atoms born inside the TS will be cool but have high radial velocity components. They make a so-called neutral SW. The secondary atoms born in the heliosheath (the SW region between the TS and HP, HS) are hot, but have low bulk speed. Because of the large charge-exchange mean free path, both populations of secondary neutral atoms can easily propagate back into the LISM and affect its properties to distances of 500–1000 AU in the upwind direction (Gruntman 1982). Therefore, the pristine LISM becomes heated and decelerated by these secondary atoms via charge exchange. This is why, even if it is superfast magnetosonic at very large distances, there may be no bow shock in the LISM in front of the HP (see Fig. 1), at least in certain radial directions. The presence of

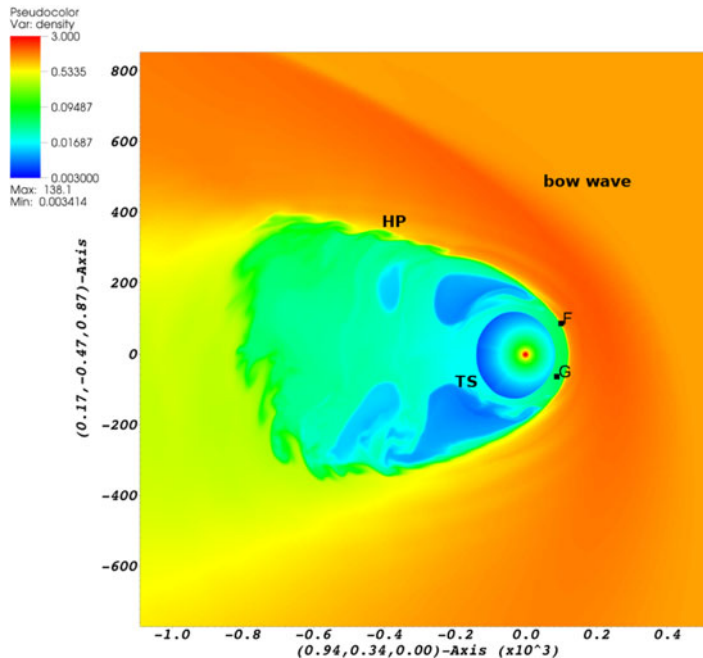


Figure 1. The picture of the SW–LISM interaction is shown through the plasma density distribution in the plane formed by the $V1$ and $V2$ trajectories. Letters F and G show the spacecraft positions in 2015. While the HP crossing distance at $V1$ is closely reproduced, we also predicted that $V2$ may cross the HP at a close distance. [From Pogorelov et al. (2015) with permission of the American Astronomical Society.]

the heliosphere affects the LISM plasma to much larger distances in the heliotail region. Moreover, ions of different energies are affected differently (e.g., PeV galactic cosmic rays, GCRs, may be affected to distances of the order of 1 pc), which makes it difficult to establish the part of the LISM modified by the heliosphere exactly. It is for this reason, Fraternali & Pogorelov 2021 proposed to extend the term Very Local Interstellar Medium (VLISM) to the LISM affected by the presence of the heliosphere, regardless of what physical processes are responsible for such modification and which physical quantities are affected. The space filled by the VLISM is sometimes called the outer heliosheath (OHS).

The secondary ions born in the SW due to charge exchange are quickly isotropized, but never reach the state of thermodynamic equilibrium (Vasyliunas & Siscoe 1976). These non-thermal ions are also called pickup ions (PUIs). They carry the majority of SW thermal energy starting from distances of the order of 10 AU and extending to the HP itself. We loosely distinguish the inner and outer heliosphere (IH and OH) by assuming that the former starts at some critical, Sun-centered sphere with radial velocity component exceeding the fast magnetosonic speed and ends when the effect of PUIs on the SW flow becomes noticeable. The OH extends to the HP itself. Pickup protons co-move with the thermal protons in the direction of the HP (Parker 1963). The effect of ion, especially PUI, streaming along magnetic field lines cannot be excluded, but it is likely limited by scattering in the turbulent magnetic field. It is worthwhile to mention that the mere applicability of the MHD treatment of collisionless SW plasma relies upon such scattering. Since the thermal energy of PUIs is high and they can experience charge exchange themselves, newly born atoms are called energetic neutral atoms (ENAs). PUIs can also be born in the OHS behind the HP, where they ultimately give birth to new ENAs. Those ENAs which are

born in the HS and OHS can propagate back to Earth, where they are measured by the *Interstellar Boundary Explorer* (McComas et al. 2017b), *Cassini/INCA* (Krimigis et al. 2009), and *Solar Heliospheric Observatory* (SOHO/HSTOF) (Hilchenbach et al. 1998; Czechowski et al. 2006). Since ENAs carry information about PUIs throughout the SW–LISM interaction region, they are used as a tool to describe the global structure of the heliosphere (Reisenfeld et al. 2021). This information is enhanced by in situ measurements performed by near-Earth spacecraft and *Voyager* 1 and 2, which crossed the TS and HP and are performing measurements in the VLISM (Stone et al. 2005, 2008, 2013, 2019). More recent, *New Horizons* (NH) mission is measuring the PUI and thermal SW properties at distances now exceeding 40 AU (McComas et al. 2017a), where PUIs are energetically dominant. *Interstellar Mapping Probe* (IMAP) is a new NASA mission, to be launched in 2024. It will perform ENA and PUI measurements with even higher accuracy (McComas et al. 2018).

More details of what has been described in this brief introduction can be found in the review papers (e.g., Bzowski et al. 2009; Izmodenov et al. 2009; Pogorelov et al. 2009, 2017b; Zank 1999, 2015).

The abundance of in situ data and remote observations makes numerical simulations challenging. Their predictive power is strongly constrained by observations and mostly applies to the regions lacking in situ measurements. For example, both *Voyagers* move into the nose of the SW–LISM interaction region. On the other hand, *IBEX* measurements of ENA fluxes are lacking those created at distances exceeding 500 AU into the heliotail. It is therefore virtually impossible to constrain the heliotail length and structure by data only. Although all numerical simulations based on identical models and physical boundary conditions give agreeable results, controversies are still possible on the border of model applicability. As far as in situ measurements are concerned, they are performed at one point per time and remain therefore incomplete as far as the global time-dependent picture is concerned.

In the following sections, a number of challenges are described that affect predictive capabilities of numerical modeling. Physical phenomena accompanying the SW–LISM interaction are so broad that many of them are applicable to various astrophysical objects, especially those involving wind–wind interactions.

2. Challenges in numerical modeling of the SW–LISM interaction

The challenges to be discussed can be separated into two categories. Firstly, it is important to choose a proper physical model. Secondly, any model should be accompanied by appropriate, typically time-dependent, boundary conditions. While ideal MHD models are commonly used to describe the SW and LISM plasma flow, the former is collisionless. The applicability of fluid equations is justified by ion scattering on magnetic field fluctuations abundant in the SW. On the other hand, p–H charge exchange mean free path is at least of the order of characteristic distances in the interaction region (e.g., the measured distance between the TS and HP is about 35 AU), so the transport of neutral atoms should be modeled kinetically (Baranov & Malama 1993). This does not mean that simpler models, where different populations of neutral atoms are treated gas dynamically, cannot be used (see a comparison of these models in Pogorelov et al. 2009).

2.1. Data-driven boundary conditions

To simulate the SW behavior, it is necessary to identify a set of boundary conditions (b.c.'s). Remote observations of the solar magnetic field are made routinely in the photosphere. These data can be used as boundary conditions for solar coronal models that

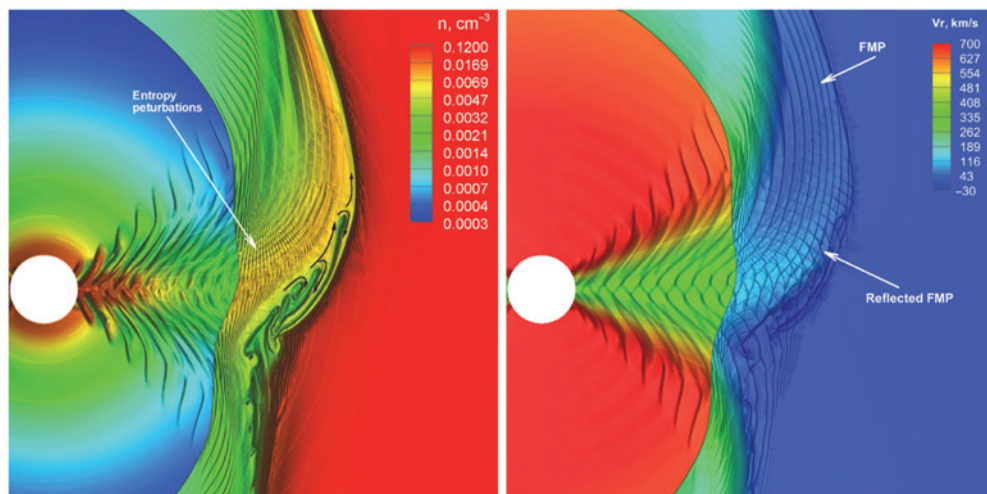


Figure 2. The only data-driven simulation of the CIR effect on the HS. Density (left panel) and radial component of the velocity (right panel) distributions in the meridional plane for the Solar Cycle 22 minimum. The entropy and fast magnetosonic perturbations (FMPs) are shown. The black arrows show the slow wind flow directions. [From Borovikov et al. (2012) with permission of the American Astronomical Union.]

propagate the SW beyond the critical sphere. In other words, solutions to the SW–LISM interaction can be driven and validated by data.

To perform meaningful comparison with data at least the following observational issues should be addressed:

- Better shock identification algorithms to be developed especially for the HS data.
- A systematic search for the sectors and sector boundaries should be performed beyond the TS. Theoretical explanations should be provided for their presence and apparent occasional destruction possibly through local magnetic reconnection.
- SW and OHS observations should be used for theoretical studies of the formation of pressure fronts and their breaking.
- Relatively high-frequency, quasi-periodic structures have been observed in the HS. Their nature and origin should be revealed.
- The SW, including the one in the HS, is a driven, open dynamical system, and the appropriate statistical mechanics is that of Tsallis (2009). The q-triplet seems to be a universal characteristic of the system. Since the Tsallis statistics is associated with the Lorentzian distribution suitable for the mixture of thermal ions and PUIs, much could be learned from this approach, particularly on relatively small scales.
- Many corotating interaction regions (CIRs, Fig. 2), merged interaction regions (MIRs), and global MIRs (GMIRs, Fig. 3), associated with a decrease in the Galactic cosmic ray (GCR) intensity, have been observed in the HS. This is why, cosmic ray data should be involved in the data analysis.
- The question to be answered by combining observations and simulations is about why MIRs and GMIRs survive out to near the HP. In addition, no numerical model is able to reproduce V_2 data in the HS satisfactorily (e.g., Fig. 4). Models that extend from the Sun through the HS are suitable for addressing these questions.

Our own Multi-Scale Fluid-Kinetic Simulation Suite (MS-FLUKSS, Pogorelov et al. 2014) is used to perform simulations of the SW flow and its interaction with the LISM with the b.c.'s at 20–25 solar radii provided to us by the well-developed POT3D-WSA coronal model constrained by remote and in situ SW observations (Arge et al. 2013;

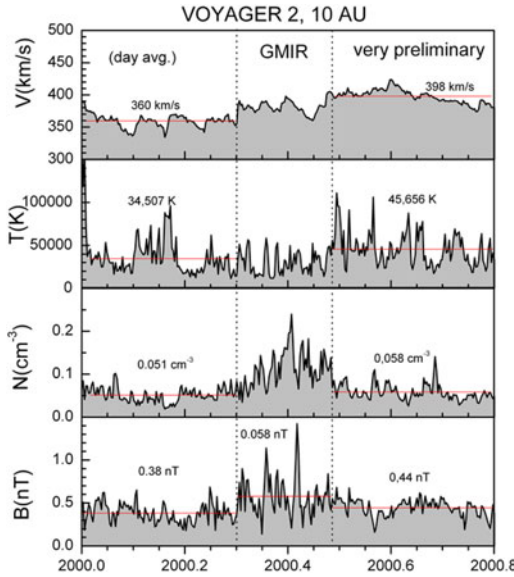


Figure 3. Quantity distributions in a typical GMIR observed by *V2*. The data is shifted by 234 days towards 10 AU.

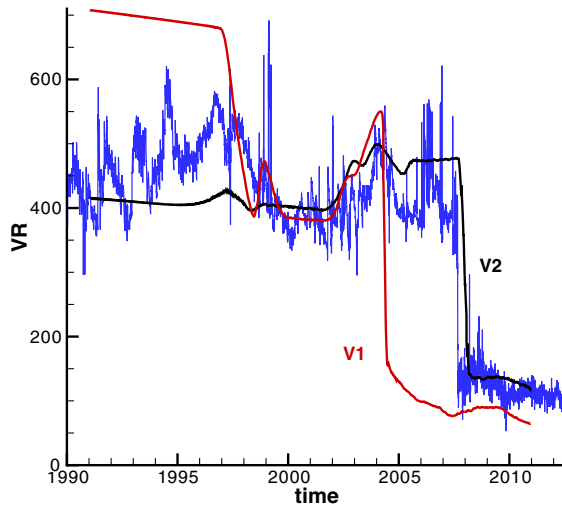


Figure 4. Radial component of the SW velocity vector along the *V2* (black line) and *V1* (red line) trajectories. *V2* observations are shown with the blue line. [From Pogorelov et al. (2013) with permission of the American Astronomical Society.]

Caplan et al. 2021). The inner b.c.'s for the ambient SW are being transferred with MHD simulations to the Earth's orbit with the uncertainty quantification (UQ) based on the WSA predictive metrics. The properties of a selected few *Voyager*- and *NH*-directed coronal mass ejections (CMEs) are derived from publicly available remote observations made by *SDO* AIA and HMI, *STEREO* A & B COR2 and H1/H2, and *SOHO* C2/C3 instruments. An additional UQ analysis is performed of the solution dependence on the observationally-derived CME properties at injection sites. *Parker Solar Probe* (*PSP*), *OMNI*, and *Ulysses* (*SWOOPS* and *SWICS*) data can be used for validation in the IH. In the OH, *Voyager* (*MAG* and *PLS*) and *NH* *SWAP* data can be engaged.

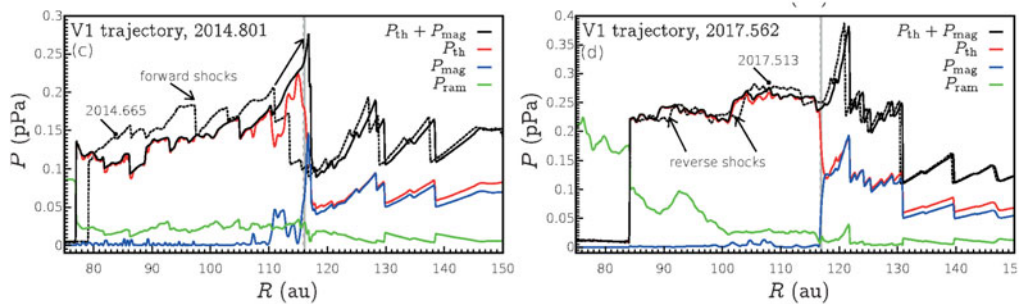


Figure 5. Two time frames with the pressure distributions along the *V1* trajectory show the forward and reverse shocks propagating through the HS. The dashed lines correspond to slightly shifted moments of time. One can also see shocks merging beyond the HP, the position of which is shown with vertical lines.

If PUIs are treated as a separate fluid, the mixture of thermal and non-thermal ions in the SW can be modeled in the assumption of different kappa distribution functions, which makes it possible, to perform a UQ based on this important parameter. The UQ analysis can be done on the basis of error propagation from 1 AU through the heliosphere.

We build our research approach on the historically proven idea that theory and numerical simulations are of immense importance for the interpretation of observational data. The latter, while providing us with the ground truth about the physical processes occurring in the heliosphere, highly benefit from the capability of modeling to experiment with the boundary conditions, switch on and off different processes, and provide global solutions. Such global solutions are especially important if they are time-dependent and account for the realistic space dimension of the problem.

The b.c.'s in the unperturbed LISM are typically derived from the He atom measurements (McComas et al. 2015), especially those atoms that experience no charge exchange on the way to 1 AU. They give us the velocity components and temperature of the LISM. The prior estimates are currently being re-analyzed because the distribution function of pristine He atoms becomes anisotropic at 1 AU. (Wood et al. 2019; Swaczyna et al. 2020; Fraternali et al. 2021). The atom (H and He) and proton densities remain uncertain and are partially derived from the SW–LISM simulation results.

In situ measurements are typically made at each individual point and time and therefore may hide the actual complexity of a phenomenon. As shown in Fig. 5a, the numerical simulation from (Pogorelov et al. 2021) makes it possible not only to identify forward and reverse shocks in the HS, but also see their evolution in time. In addition, one can see overtaking of shocks propagating upstream in the LISM – the phenomenon so infrequent that it can hardly be observed by a single spacecraft.

Another surprising observation (Stone et al. 2008) was that *V2* crossed the TS at a much smaller heliocentric distance than *V1* (84 AU against 94 AU). While a number of possible explanations were proposed, some entirely unrealistic, the simulation of Pogorelov et al. (2013) driven by *Ulysses* measurement reproduced both the crossing time and the corresponding stand-off distances (see Fig. 4).

Pogorelov et al. (2021) show that time-dependent and data-driven numerical simulations can reproduce a surprising absence of the magnetic field rotation across the HP observed both by *V1* and *V2* (Burlaga et al. 2019).

2.1.1. An empirically driven solar wind model

The outer atmosphere of the Sun, the solar corona, is a plasma that expands to become the supersonic SW, which envelopes the planets and forms the heliosphere. The SW structure and dynamics are strongly influenced by the solar magnetic field, including the locations of fast and slow SW, and the position of the heliospheric current sheet (HCS). The magnetized SW is also the primary medium by which solar activity is transmitted to Earth and beyond, in the form of CMEs, which evolve and propagate in the wind, and energetic particles, which are transported with the magnetic field. The solar magnetic field is therefore a key component in any predictive SW model.

Empirical models are able to predict SW structure with reasonable success from a magnetic field model based on photospheric magnetic field maps (Riley et al. 2021). The OH evolves over long time periods compared to the solar rotation time scale. To model the global heliosphere over many years, we need to capture the large-scale evolution of the SW which is driven by changes in the solar magnetic field. We require a physically consistent description of the photospheric flux evolution that is continually updated. The processes by which the magnetic flux on the Sun evolves have been studied for many years. Assimilative Surface Flux Transport (SFT) models incorporate these processes (primarily differential rotation, meridional flow, supergranular diffusion, and random flux emergence) and have been successful in predicting the evolution of photospheric magnetic fields. Presently available models include the LMSAL Evolving Surface-Flux Assimilation Model (Schrijver & De Rosa 2003), the ADAPT model (Arge et al. 2013), and the Advective Flux Transport model (AFT) (Upton & Hathaway 2014). The map sequences provided by these models can be used to drive time-dependent, empirically driven MHD SW models that approximate its long-term evolution.

2.1.2. Coronal mass ejections and their uncertainty quantification

We have implemented two flux rope models in MS-FLUKSS: a modified spheromak model (Singh et al. 2020a,b) and a constant turn model based on FRiED model geometry (Isavnin 2016). Both can be initiated with desired speed, direction, orientation, mass, poloidal and toroidal magnetic fluxes, and a helicity sign. The initial kinematic and magnetic properties of CMEs are derived from various observations. We use the graduated cylindrical shell (GCS) model (Thernisien et al. 2009) to estimate CME speed, direction, and orientation using multiple viewpoint images from *STEREO* and *SOHO* coronagraphs. CME mass is calculated using the bright light coronagraph observations (Colaninno & Vourlidas 2009). The poloidal flux of CMEs is calculated from the reconnected flux under the post-eruption arcades (PEAs) (Gopalswamy et al. 2018; Singh et al. 2019). The toroidal flux of CMEs is calculated from coronal dimming at the CME footprints (Dissauer et al. 2019; Singh et al. 2020a). If there is no coronal dimming during a CME eruption, the toroidal flux can be estimated using the empirical relation between the toroidal and poloidal fluxes (Qiu et al. 2007). The helicity sign of CME flux ropes can be determined from magnetic field distribution in the source active regions (Luoni et al. 2011). All these parameters have observational errors associated with their estimates. This means that ensemble modeling of CMEs can be performed to get estimates about the uncertainties in CME simulations by creating ensemble members according to the expected errors in the initial CME model parameters.

2.2. Pick up ions crossing the termination shock. The width of the heliosheath

Although the SW plasma consists of the thermal SW ions and PUIs, we choose to solve the MHD system for the plasma mixture in the conservation-law form because

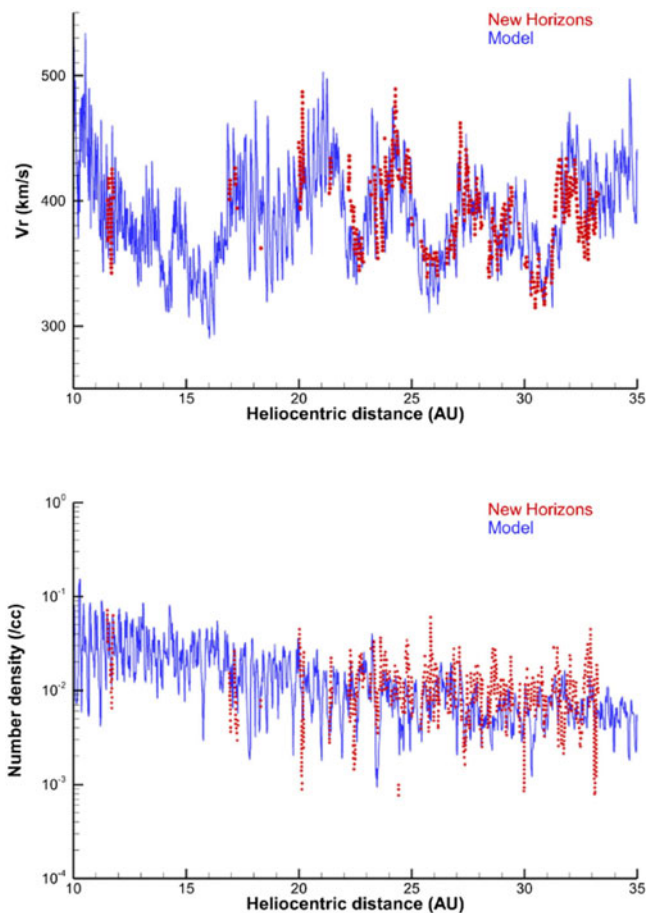


Figure 6. Radial velocity component and number density compared to the daily averaged *NH* SWAP data. [From Kim et al. (2016) with permission of the American Astronomical Society].

this allows us to satisfy the conservation laws of mass, momentum, energy, and magnetic flux at the TS efficiently. Clearly, some assumptions should be made about the distribution functions of protons and PUIs. It is usually assumed that the SW protons are Maxwellian. This is not true for PUIs. Zank et al. (2010) showed that assuming a kappa distribution for the mixture makes it possible to approximate the realistic distribution function. Heerikhuisen et al. (2019); DeStefano & Heerikhuisen (2017, 2020) studied the effect of the distribution function on the charge exchange source terms. The kappa distribution decreases the contribution of the most probable state while increasing the number of ions in the so-called “energetic tails.” The important conclusion derived from DeStefano & Heerikhuisen (2017, 2020) is that the dependence of charge-exchange cross-sections on energy should be preserved when the integration is performed. This becomes crucial for κ approaching the minimum allowed value of $3/2$. If this procedure is not followed, the effect of PUIs on the heliosphere is substantially exaggerated (Heerikhuisen et al. 2015).

We are using two approaches to take into account PUIs: (1) PUIs are not treated as a separate plasma component, but the conservation of mass, momentum, and energy for the mixture is preserved, while the solution dependence on the value of κ is investigated; (2) some sort of an isotropic distribution function for PUIs away from the TS is chosen,

they are assumed to be co-moving with the SW ions, and the continuity and pressure equations are solved to describe the PUI flow (Pogorelov et al. 2016). The latter approach is easier to implement in the supersonic SW inside the TS (see, e.g., Kim et al. 2016). Figure 6 shows the comparison of our simulation based on model 2 with *NH* observations.

The description of PUIs crossing collisionless shocks, such as the TS, is impossible with the MHD, ideal or dissipative, approaches, because the details of kinetic shock structure, like the overshoot, are responsible for PUI reflections into the upstream region. Some kind of modified Rankine–Hugoniot-type boundary conditions describing the PUI transition across the TS are required. The fluid descriptions of the TS crossings by PUIs have been made so far either with simplified shock conditions (Pogorelov et al. 2016; Wu et al. 2016; Kornbleuth et al. 2020) or no conditions at all (Usmanov et al. 2016). Gedalin et al. (2020, 2021a,b) performed an extensive, probabilistic, test-particle simulations to derive such b.c.'s. The results have been validated with full-PIC simulations. It has been shown that the fraction of initially reflected PUIs is larger than that derived from the estimates involving only the cross-shock potential effect. In addition, the downstream perpendicular temperature of reflected PUIs appeared to be an order of magnitude lower than it was proposed by Chalov & Fahr (2000) and Zank et al. (2010).

The discussion of the HS width is complicated by the absence of in situ measurements for the TS and HP distances from the Sun at the same moment of time. Pogorelov et al. (2015) predicted that *V2* should cross the HP at a distance very close to that of *V1*. A separate treatment of PUIs indeed decreases the HS width (Pogorelov et al. 2016). However, data-driven numerical simulations reported by Kim et al. (2017) and Pogorelov et al. (2021), where PUIs were not treated separately, showed this width is variable: it has been smaller than 40 au since about 2014, reached 30 au in 2017, and now remains almost constant (about 35 au) in the *V1* direction. This is rather close to the difference between the observed crossings of the TS and HP.

2.3. The effect of magnetic field dissipation on the thermodynamic properties and velocity of the SW in the IHS

The HMF becomes almost radial at 0.1 au from the Sun. However, the regions of positive and negative polarity are separated by a current-carrying surface, which is called the heliospheric current sheet (HCS). Due to the Sun's rotation, the HMF lines acquire spiral shape. However, the Sun's magnetic and rotation axes do not coincide. For this reason, the idealized HCS, for the tilt between the Sun's magnetic and rotation axes (equal to 35°) acquires a complex shape shown in Fig. 7 (*left panel*). In reality, this shape is not preserved beyond ~ 10 au because of the SW flow asymmetries and stream interaction. However, the width of each magnetic field sector decreases with decrease of the SW speed and vanishes near the SW stagnation point on the HP surface. In practice, this means that the sector structure cannot be resolved in its entirety for any chosen grid resolution. While one would expect some sort of numerical dissipation of the HMF in this case, the HMF strength starts to oscillate exhibiting the features of stochastic behavior, if the grid resolution is sufficiently high, (Fig. 7, *right panel*). *Ulysses* data driven simulations presented by Pogorelov et al. (2013) show that the calculated value of the (dominant) transverse HMF component is of the order of 1 μG , which is close to the average value of the same, strongly oscillating component in observations. In principle, magnetic field dissipation should result in the SW heating and its slower deceleration. Unfortunately, identification of such features in the turbulent SW behind the TS is a challenging task, which is still to be undertaken.

An approach proposed by Czechowski et al. (2010) and Borovikov et al. (2011) was based on the idea that the HMF can be assumed unipolar in numerical simulations while

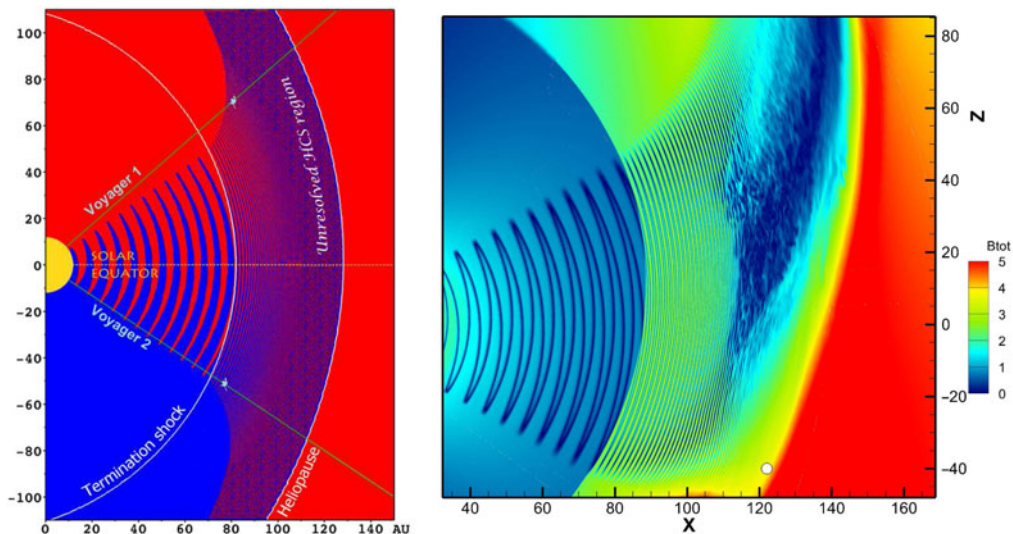


Figure 7. (Left panel) The HCS is shown using the boundary between the positive (red color) and negative (blue color) polarities tracked by the level-set method in the assumption of unipolar HMF. (Right panel) The distribution of the magnetic field magnitude with the Parker HMF distribution at the inner boundary. Transition to stochastic behavior occurs in the region where the HCS is no longer resolved. [From Borovikov et al. (2012) and Pogorelov et al. (2015) with permission of the American Astronomical Society.]

the magnetic field polarity is assigned after each time step by tracing the HCS shape with a level-set method. However, this approach turned out to have two major deficiencies. Firstly, even the level-set equation sooner or later stops to resolve the sector structure. Secondly, the HMF strength becomes unrealistically strong (Izmodenov & Alexashov 2020; Pogorelov et al. 2017a, 2021), which disagrees with *Voyager* data by a factor of ~ 7 . Moreover, the plasma beta becomes less than 1 in the HS, so the SW flow gets under control of magnetic pressure, which can collimate the flow in the heliotail (Yu 1974). The collimation occurs inside the Parker field branches spiraling into the tail region. In the extreme case of unipolar HMF, such spiraling can result into the heliotail splitting into two branches (Opher et al. 2015; Pogorelov et al. 2015). Such splitting disappears even in the assumption of a flat HCS, which happens when the Sun's magnetic and rotation axes coincide. Moreover, the reasons for the collimation disappear because of the "kinking" or "sausage" instabilities. Moreover, the solar cycle effects, especially the presence of the dense, slow and rarefied, fast SW regions with the variable latitudinal extent of the boundary between them completely destroys the artificial collimation, in this way removing the possibility of split-tail structures.

2.4. Magnetic field behavior at the heliopause

Pogorelov et al. (2021) show that time-dependent and data-driven numerical simulations can reproduce a surprising absence of the magnetic field rotation across the HP observed both by *V1* and *V2* (Burlaga et al. 2019).

It is worth noting, however, that the behavior of magnetic field vectors across the HP along *V1* and *V2* trajectories cannot be reproduced with the boundary conditions assuming the unipolar HMF. The reasons are on the surface. As seen from Pogorelov et al. (2015, 2021); Izmodenov & Alexashov (2020), and Opher et al. (2020), the magnetic field strength is practically continuous across the HP in the assumption of unipolar HMF.

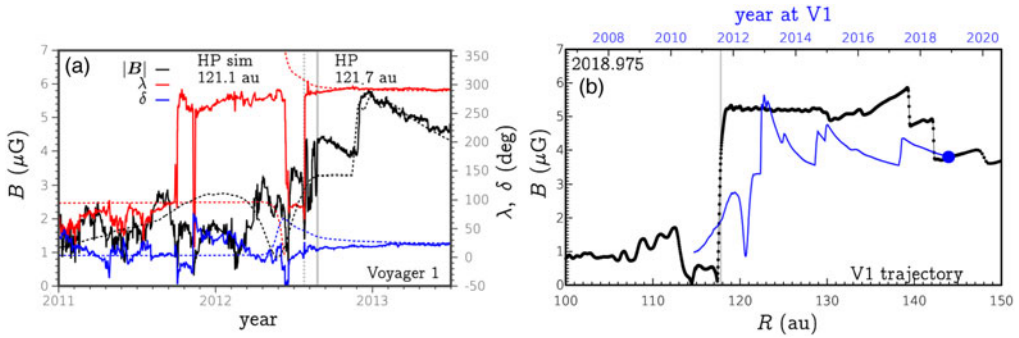


Figure 8. (Panel (a)) The magnetic field strength, and its elevation and azimuthal angles in the vicinity of the HP crossing measured by *Voyager 1* (solid lines) and simulated in Kim et al. (2017) (dashed lines). The vertical lines show the HP position at the moment of *V1* entering the LISM. (Panel (b)) Two shocks approaching each other before merging in the OHS. The blue line shows the magnetic field distribution at a virtual *V1* propagating through the solution. [Adapted from Pogorelov et al. (2021) with permission of the American Astronomical Society.]

Since the HP is a tangential discontinuity, the equality of magnetic pressures across it can be satisfied only if the magnetic pressure dominates over the thermal pressure. This is in accord with our explanation of the exaggerated SW collimation inside the Parker field spirals bent into the heliotail.

2.5. Propagation of waves and shocks through the VLISM, and their interaction. The structure of collisional shocks in the LISM

Data-driven simulation of the SW-LISM interaction (Kim et al. 2017; Pogorelov et al. 2021) show that some of the shocks observed by *V1* can be well reproduced. It was also shown that each shock created at the HP and propagating upstream into the LISM decreases in intensity and speed as it propagates radially outward, and ultimately disappears at some distance from the HP. A shock can become stronger only when one shock overtakes another. Such shock interaction is shown in Fig. 8b of the magnetic field distribution along the *V1* trajectory, where we show both the time frames and the quantities taken by a virtual probe (indicated at each moment of time with a blue circle) co-moving with the *V1* along its trajectory.

In Fig. 8a, we present the distribution of $|\mathbf{B}|$, and its elevation and azimuthal angles, δ and λ , as a function of time along the *V1* trajectory. The observational data and simulation results are shown with solid and dashed lines, respectively. Although the simulated distributions are not in full agreement with the observations, one can see that δ and λ are continuous across the HP, which is shown with the vertical lines. Their values asymptotically approach those observed by the spacecraft.

2.6. The nature of the density increase beyond the heliopause

The increase in the plasma wave frequency observed by the *Voyager* Plasma Wave Instrument (PWS) has been of substantial interest for a long time. This increase implies that the plasma density is also increasing, on the average, with distance from the HP, i.e., the density maximum is not at the surface of the HP itself. The first two explanations for that phenomenon were proposed by Gurnett et al. (2015) and Cairns & Fuselier (2017). The former explanation is simply a misinterpretation of numerical simulations. The early, low-accuracy, discontinuity-capturing simulations resulted in a very wide dissipative structure of the HP (Steinolfson et al. 1994). This means that the density profile

looked rather wide and smooth. If one identifies the position of the HP in a chosen direction as the point where the density profile has maximum gradient, the maximum of the density itself reveals itself as some distance from the HP. However, the numerical width of the HP cannot be as large as 40–50 au, which is the observed distance of the continuing increase in the plasma density. The current analysis of numerical simulations where the surface of the HP was fitted exactly, like those in Baranov & Malama (1993), showed that the density increase behind the HP should be separated from the sharp increase across the HP as a discontinuity. This phenomenon was also reconfirmed by the high-resolution, discontinuity-capturing simulations of Pogorelov et al. (2017a). The second explanation appealed to the magnetic-field induced anisotropies in the VLISM plasma. While the absence of such anisotropies cannot be excluded or confirmed by *Voyager* data, it is clear that the phenomenon exists even in the absence of magnetic field (Baranov & Malama 1993). Pogorelov et al. (2017a) suggested that this density increase is somehow related to the process of charge exchange in the VLISM. The argument in favor of such explanation was the similarity in the model-derived density-increase width with the proton-H atom mean free path. However, Pogorelov et al. (2021) pointed out that the density should not be expected to have maximum at the HP surface. By analogy with the supersonic blunt body problem, it is clear that this never happens, except for the critical streamline directed into the stagnation point on the HP surface.

2.7. Plasma wave generation in the VLISM and its relationship to the Alfvén velocity distributions along the Voyager trajectories newly derived from the spacecraft data

The subject discussed in the previous section is intimately related with the distribution of the Alfvénic velocity along the *V1* and *V2* trajectories in the VLISM. There is a close association between the electron plasma oscillations (Gurnett et al. 2013) and the jumps in the magnetic field strength Burlaga et al. (2013) observed in the OHS. According to PWS measurements (Gurnett et al. 2015), *V1* observed radio emission in the 2–3 kHz range, which is thought to be excited by shocks propagating through plasma regions primed with nonthermal electrons resonantly accelerated by lower hybrid (LH) waves driven by a ring-beam instability of PUIs (Gurnett et al. 1993; Cairns & Zank 2002). Further acceleration of these electrons by a propagating shock may create electron beams moving away from it. These beams produce Langmuir waves, via the “bump-on-tail” instability (Filbert & Kellogg 1979; Cairns 1987). For a shock front convex outward with respect to the incoming plasma flow, the bump-on-tail velocity distribution is due to the existence of a threshold velocity below which electrons cannot reach a given point upstream of the shock. The region accessible to such beams is called the electron foreshock. The presence of nonthermal electrons is insufficient for the development LH instability. The instability growth rate and energy transfer to electrons should be sufficiently large, which occurs (see Cairns & Zank 2002 and references therein) if $\alpha_r = V_r/V_A < 5$, where V_r and V_A are the PUI ring-beam and Alfvén velocities, respectively. Magnetic field draping around the HP creates conditions for larger V_A . For PUIs born in the OHS by charge exchange of the VLISM ions with the neutral SW, which actually have a ring-beam distribution, V_r should be ~ 400 km/s.

Voyager data provide us with a new perspective on the plasma wave and radio emission generation. The analysis of these data in Pogorelov et al. (2021) showed that V_A decreases with distance from the HP, and is below 45 km/s at *V1* and 85 km/s at *V2* immediately after the HP. The Alfvénic velocity increases across the shocks traversing the OHS, but not substantially, since all shocks observed in that region so far have been rather weak. It is therefore unlikely that α_r would be smaller than 5 for ring-beam velocities corresponding to the neutral SW. For this reason, there remains a question about the

physical mechanisms responsible for the plasma wave and radio emission generation on the OHS, since Roytershteyn et al. (2019) reported no substantial LH instability for a realistic, three-component distribution of PUIs beyond the HP.

3. Conclusions

This paper presented a number of observational phenomena that benefited from numerical simulations. Such simulations help understand in situ data obtained by an individual, or even two individual spacecraft, such as *V1* and *V2*. This is because one point in space per time observations may and do hide the details of stream and shock interaction. Of interest for large-scale simulations is the data analysis the VLISM turbulence performed by Fraternali & Pogorelov (2021). It was found, in particular, that the dissipative width of observed shock structures is too narrow to be attributed to Coulomb collisions alone. Moreover, high variability of the shock width structures suggests that that no actual shocks are observed in the collisional VLISM. Instead, *Voyagers* are crossed by sharp gradients which have not sufficient time to break in the turbulent plasma accompanied by transient wave activity.

Acknowledgement

This work was supported in part by NASA grants 80NSSC19K0260, 80NSSC18K1649, 80NSSC18K1212, and NSF-BSF grant PHY-2010450. It was also partially supported by the *IBEX* mission as a part of NASA's Explorer program. The authors acknowledge the Texas Advanced Computing Center (TACC) at The University of Texas at Austin for providing HPC resources on Frontera supported by NSF LRAC award 2031611. Supercomputer time allocations were also provided on SGI Pleiades by NASA High-End Computing Program award SMD-17-1537 and Stampede2 by NSF XSEDE project MCA07S033.

References

- Arge, C. N., Henney, C. J., Hernandez, I. G., et al. 2013, in AIP Conference Series, Vol. 1539, Solar Wind 13, ed. G. P. Zank & et al., 11–14
- Baranov, V. B., & Malama, Y. G. 1993, JGR, 98, 15157
- Borovikov, S. N., Pogorelov, N. V., Burlaga, L. F., & Richardson, J. D. 2011, ApJL, 728, L21
- Borovikov, S. N., Pogorelov, N. V., & Ebert, R. W. 2012, ApJ, 750, 42
- Burlaga, L., Ness, N. F., Berdichevsky, D., et al. 2019, Nature Ast., 3, 1007
- Burlaga, L. F., Ness, N. F., Gurnett, D. A., & Kurth, W. S. 2013, ApJL, 778
- Bzowski, M., Mobius, E., Tarnopolski, S., Izmodenov, V., & Gloeckler, G. 2009, SSR, 143, 177
- Cairns, I. H. 1987, JGR, 92, 2329
- Cairns, I. H., & Fuselier, S. A. 2017, ApJ, 834, 197
- Cairns, I. H., & Zank, G. P. 2002, Geophys. Res. Lett., 29, 47
- Caplan, R. M., Downs, C., Linker, J. A., & Mikic, Z. 2021, ApJ, 915, 44
- Chalov, S. V., & Fahr, H. J. 2000, A&A, 360, 381
- Colaninno, R. C., & Vourlidas, A. 2009, ApJ, 698, 852
- Czechowski, A., Hilchenbach, M., Hsieh, K. C., Kallenbach, R., & Kóta, J. 2006, ApJL, 647, L69
- Czechowski, A., Strumik, M., Grygorczuk, J., et al. 2010, A&A, 516, A17
- DeStefano, A. M., & Heerikhuisen, J. 2017, in J. Phys. Conf. Ser., Vol. 837, 012013
- DeStefano, A. M., & Heerikhuisen, J. 2020, Physics of Plasmas, 27, 032901
- Dissauer, K., Veronig, A. M., Temmer, M., & Podladchikova, T. 2019, ApJ, 874, 123
- Filbert, P. C., & Kellogg, P. J. 1979, JGR, 84, 1369
- Fraternali, F., & Pogorelov, N. V. 2021, ApJ, 906, 75
- Fraternali, F., Pogorelov, N. V., & Heerikhuisen, J. 2021, ApJL, 921, L24
- Gedalin, M., Pogorelov, N. V., & Roytershteyn, V. 2020, ApJ, 889, 116

- . 2021a, *ApJ*, 910, 107
- . 2021b, *ApJ*, 916, 57
- Gopalswamy, N., Akiyama, S., Yashiro, S., & Xie, H. 2018, *JASTP*, 180, 35
- Gruntman, M. A. 1982, *Soviet Astronomy Letters*, 8, 24
- Gurnett, D. A., Kurth, W. S., Allendorf, S. C., & Poynter, R. L. 1993, *Science*, 262, 199
- Gurnett, D. A., Kurth, W. S., Burlaga, L. F., & Ness, N. F. 2013, *Science*, 341, 1489
- Gurnett, D. A., Kurth, W. S., Stone, E. C., et al. 2015, *ApJ*, 809
- Heerikhuisen, J., Zirnstein, E., & Pogorelov, N. 2015, *JGR*, 120, 1516
- Heerikhuisen, J., Zirnstein, E. J., Pogorelov, N. V., Zank, G. P., & Desai, M. 2019, *ApJ*, 874, 76
- Hilchenbach, M., Hsieh, K. C., Hovestadt, D., et al. 1998, *ApJ*, 503, 916
- Isavnin, A. 2016, *ApJ*, 833, 267
- Izmodenov, V. V., & Alexashov, D. B. 2020, *A&A*, 633, L12
- Izmodenov, V. V., Malama, Y. G., Ruderman, M. S., et al. 2009, *SSR*, 146, 329
- Kim, T. K., Pogorelov, N. V., & Burlaga, L. F. 2017, *ApJL*, 843
- Kim, T. K., Pogorelov, N. V., Zank, G. P., Elliott, H. A., & McComas, D. J. 2016, *ApJL*, 832, 72
- Kornbleuth, M., Opher, M., Michael, A. T., et al. 2020, *ApJL*, 895, L26
- Krimigis, S. M., Mitchell, D. G., Roelof, E. C., Hsieh, K. C., & McComas, D. J. 2009, *Science*, 326, 971
- Luoni, M. L., Démoulin, P., Mandrini, C. H., & van Driel-Gesztelyi, L. 2011, *Solar Physics*, 270, 45
- McComas, D. J., Bzowski, M., Fuselier, S. A., et al. 2015, *ApJS*, 220, 22
- McComas, D. J., Zirnstein, E. J., Bzowski, M., et al. 2017a, *ApJS*, 233, 8
- . 2017b, *ApJS*, 229, 41
- McComas, D. J., Christian, E. R., Schwadron, N. A., et al. 2018, *SSR*, 214, 116
- Opher, M., Drake, J. F., Zieger, B., & Gombosi, T. I. 2015, *ApJL*, 800
- Opher, M., Loeb, A., Drake, J., & Toth, G. 2020, *Nature Ast.*, 4, 675
- Parker, E. N. 1963, *Interplanetary dynamical processes* (Interscience Publishers)
- Pogorelov, N. V., Bedford, M. C., Kryukov, I. A., & Zank, G. P. 2016, *J. Phys. Conf. Series*, 767
- Pogorelov, N. V., Borovikov, S., Heerikhuisen, J., et al. 2014, in *Proc. 2014 Ann. Conf. on Extreme Science and Engineering Discovery Environment, XSEDE '14*, 22:1–22:8
- Pogorelov, N. V., Borovikov, S. N., Heerikhuisen, J., & Zhang, M. 2015, *ApJL*, 812
- Pogorelov, N. V., Fraternali, F., Kim, T. K., Burlaga, L. F., & Gurnett, D. A. 2021, *ApJ*, 917, L20
- Pogorelov, N. V., Heerikhuisen, J., Roytershteyn, V., et al. 2017a, *ApJ*, 845
- Pogorelov, N. V., Heerikhuisen, J., Zank, G. P., & Borovikov, S. N. 2009, *SSR*, 143, 31
- Pogorelov, N. V., Suess, S. T., Borovikov, S. N., et al. 2013, *ApJ*, 772
- Pogorelov, N. V., Fichtner, H., Czechowski, A., et al. 2017b, *SSR*, 212, 193
- Qiu, J., Hu, Q., Howard, T. A., & Yurchyshyn, V. B. 2007, *ApJ*, 659, 758
- Reisenfeld, D. B., Bzowski, M., Funsten, H. O., et al. 2021, *ApJS*, 254, 40
- Riley, P., Lionello, R., Caplan, R. M., et al. 2021, *A&A*, 650, A19
- Roytershteyn, V., Pogorelov, N. V., & Heerikhuisen, J. 2019, *ApJ*, 881, 65
- Schrijver, C. J., & De Rosa, M. L. 2003, *Solar Physics*, 212, 165
- Singh, T., Kim, T. K., Pogorelov, N. V., & Arge, C. N. 2020a, *Space Weather*, 18, e02405
- Singh, T., Yalim, M. S., Pogorelov, N. V., & Gopalswamy, N. 2019, *ApJL*, 875, L17
- . 2020b, *ApJ*, 894, 49
- Steinolfson, R. S., Pizzo, V. J., & Holzer, T. 1994, *Geophys. Res. Lett.*, 21, 245
- Stone, E. C., Cummings, A. C., Heikkila, B. C., & Lal, N. 2019, *Nature Ast.*, 3, 1013
- Stone, E. C., Cummings, A. C., McDonald, F. B., et al. 2005, *Science*, 309, 2017
- . 2008, *Nature*, 454, 71
- . 2013, *Science*, 341, 150
- Swaczyna, P., McComas, D. J., Zirnstein, E. J., et al. 2020, *Astrophys. J.*, 903, 48
- Thernisien, A., Vourlidas, A., & Howard, R. A. 2009, *Solar Physics*, 256, 111
- Tsallis, C. 2009, *Introduction to nonextensive statistical mechanics: approaching a complex world* (Springer Science & Business Media)

- Upton, L., & Hathaway, D. H. 2014, *ApJ*, 780, 5
- Usmanov, A. V., Goldstein, M. L., & Matthaeus, W. H. 2016, *ApJ*, 820, 17
- Vasyliunas, V. M., & Siscoe, G. L. 1976, *JGR*, 81, 1247
- Wood, B. E., Müller, H.-R., & Möbius, E. 2019, *ApJ*, 881, 55
- Wu, Y., Florinski, V., & Guo, X. 2016, *ApJ*, 832, 61
- Yu, G. 1974, *ApJ*, 194, 187
- Zank, G. P. 1999, *SSR*, 89, 413
- . 2015, *ARAA*, 53, 449
- Zank, G. P., Heerikhuisen, J., Pogorelov, N. V., Burrows, R., & McComas, D. 2010, *ApJ*, 708, 1092